ROYAL ACADEMY OF OVERSEAS SCIENCES

First Young Researchers Overseas' Day
16 December 2014, Brussels, Belgium

On the way to improving moderate spatial resolution ocean color data nearby highly productive Arctic ice edges

Clémence Goyens[1*], Simon Bélanger[1], Julien Laliberté[1], Marcel Babin[2]

[1]*Université du Québec à Rimouski, Rimouski, G5L 3C6, Canada*
[2]*Unité Mixte International TAKUVIK, Québec, G1V 0A6, Canada*
[*]*Corresponding Author. Email:clemence.goyens@uqar.ca*

Abstract

Phytoplankton plays a crucial role in the world carbon cycle and marine food web. However, impact of global warming on phytoplankton species composition and abundance remains uncertain. This is particularly true in the Arctic Ocean and its marginal seas where global warming tends to be the most pronounced. Ocean color satellite images therefore represent an essential tool for providing a synoptic view of marine environments at spatial and temporal resolutions that traditional sampling methods are unable to acquire. However, over icy waters the quality of satellite images is largely affected by sea ice contamination. Today, the impact of sub-pixel and adjacent sea ice floes on the satellite measured signal are ignored in standard ocean color processing chains resulting in erroneous satellite derived bio-geochemical products. Here we explain how sea-ice affects the quality of satellite ocean color data by comparing *in situ* water reflectance measurements taken near ice-edges and/or ice-floes with spatial and temporal coincident satellite retrieved water reflectance data. In addition, high and medium spatial resolution satellite data are compared to evaluate the potential to correct ocean color data from sea-ice contamination by taking advantage of the synergy between high and medium spatial resolution images.

Keywords: Arctic, Remote sensing, Ocean color, MODIS Aqua, Landsat, sea-ice contamination

DOI : http://doi.org/10.5281/zenodo.269644
Selection and peer-review under responsibility of KAOW-ARSOM Scientific Committee

1. Introduction

Phytoplankton are responsible for approximately half of the planetary primary production and play a key role in the world carbon cycle and marine food web. An in-depth understanding of their dynamics and abundance is therfeore essential, particularly in the context of ongoing global warming. Indeed, it remains unknown if subsequent ice melt will increase or decrease primary production by phytoplankton. Studies disagree about the consequences of sea ice melt on phytoplankton distribution and growth (e.g., Antoine *et al.*, 2005; Boyce *et al.*, 2010). Terrigenous organic carbon is also expected to be affected in the near future due to important river discharge, permafrost thawing and decreasing summer ice cover. This is particularly true in the Arctic region where global warming tends to be the most pronounced (Perovich *et al.*, 2012). The limited understanding of future Arctic phytoplankton and organic matter dynamics largely results from a lack of accurate data. Thus, ocean color sensors onboard satellites represent a valuable tool for providing a synoptic view of the ocean system. Satellite images allow estimation of the spectral water leaving reflectance (often referred to as the ocean color and denoted by $\rho_w(\lambda)$ where λ stands for light wavelength), which in turn provides information about phytoplankton biomass (e.g., through the use of proxies such as Chlorophyll a, Chl_a) and terrigenous material. To acquire accurate satellite $\rho_w(\lambda)$ estimates, the atmospheric contribution needs to be extracted from the sensor-measured signal, $\rho_{TOA}(\lambda)$. The atmospheric contribution may be defined as the solar radiation reflected by air molecules, $\rho_r(\lambda)$, and atmospheric aerosols, $\rho_a(\lambda)$, and by the interaction between both, $\rho_{ar}(\lambda)$, often significant in the sensor bands of interest for ocean color applications (Fig. 1).

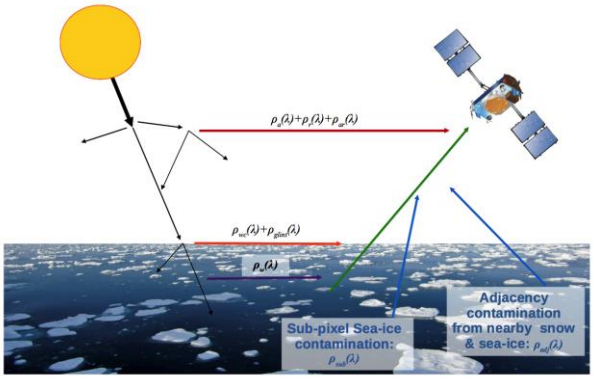

Fig. 1. Schematic overview of the atmospheric ($\rho_a(\lambda)$, $\rho_r(\lambda)$, $\rho_{ar}(\lambda)$) and sea-surface ($\rho_{wc}(\lambda)$, $\rho_{glint}(\lambda)$) contribution to the top of atmosphere sensor measured signal.

Light originating from sun glint at the air-sea interface, $\rho_{glint}(\lambda)$, and white-caps from breaking waves, $\rho_{wc}(\lambda)$, also need to be removed from the sensor-measured signal. During preprocessing, the sensor-measured signal is corrected for gas absorption, Rayleigh

scattering, white-caps and sun glint. Accordingly, if the optical properties and the concentration of the aerosols are known, $\rho_a(\lambda)$ and $\rho_{ar}(\lambda)$ can be estimated and subsequently, $\rho_w(\lambda)$. In the near infra-red (NIR) spectral region $\rho_w(\lambda)$ is generally null or can be approximated by making assumptions (e.g., Ruddick *et al.*, 2000). Hence, standard satellite data processing chains tend to estimate ρ_w(NIR) to derive the aerosol model from ρ_a(NIR) and ρ_{ar}(NIR). Next, knowing the aerosol model, $\rho_a(\lambda)$ and $\rho_{ar}(\lambda)$ can be interpolated towards the shorter wavelengths and $\rho_w(\lambda)$ can be estimated for the entire visible range. The process of estimating $\rho_w(\lambda)$ from $\rho_{TAO}(\lambda)$ is called atmospheric correction (AC).

In icy waters, the presence of sea-ice makes AC even more challenging because the quality of the data is seriously compromised due to, among others, contamination of the signal by sea ice. This is particularly true along the receding ice-edge in marginal ice zones where spring and summer phytoplankton blooms are observed. Hence, to ensure accurate $\rho_w(\lambda)$ retrievals in icy waters, the light reflected by sub-pixel and adjacent ice-floes in the direction of the satellite sensor ($\rho_{sub}(\lambda)$ and $\rho_{adj.}(\lambda)$, respectively) needs to be taken into account in the AC process. Current standard AC methods ignore both $\rho_{sub}(\lambda)$ and $\rho_{adj.}(\lambda)$ resulting in potentially important biases in the interpretation of ocean color data. Previous studies have shown that standard AC processes in presence of sub-pixel contamination tend to overestimate the contribution of aerosol and, subsequently, underestimate $\rho_w(\lambda)$ in the visible spectral bands (particularly in the blue spectral region) (Bélanger *et al.*, 2007; Wang and Shi, 2009). In contrast, $\rho_w(\lambda)$ is expected to be overestimated near ice-floes due to adjacency effect (Bélanger *et al.*, 2007). Since light scattering from air molecules is stronger at shorter wavelengths (λ^{-4}), adjacency effect from sea-ice will mostly increase the spectral reflectance of the pixel at the shorter wavelengths. To avoid this misinterpretation, methods have been suggested to mask sea-ice contaminated pixels (e.g., Bélanger *et al.*, 2007; Wang and Shi, 2009). However, the extent of the ice-contamination remains to be quantified and since most of the phytoplankton biomass develops along the receding ice-edges, masking ice contaminated pixels results in a significant loss of data and may lead to erroneous conclusions about Arctic phytoplankton and organic carbon related processes (IOCCG, 2015). There is therefore a need to develop a reliable approach to correct the ice-related contamination of remotely-sensed ocean color signals. The present study evaluates how contamination, largely from sea ice, affects the accuracy of ocean color images based on a set of time and space coincident *in situ* and satellite data (section 3.1.) as well as a visual inspection of medium and high spatial resolution images, taken simultaneously (section 3.2).

2. Data and methods

2.1. *In situ* data

To evaluate the error made by the satellite sensor in presence of sea-ice, *in situ* data from the ArcticNet 2011 sea-campaign are used. 822 above-water spectra measured with a HyperSAS instrument were processed following Mobley (1999) and Ruddick *et al.* (2006) in order to obtain $\rho_w(\lambda)$ values comparable to the satellite measured $\rho_w(\lambda)$. For most *in situ* data,

additional information about the surroundings of the measurement location is provided, allowing us to classify the *in situ* data into 5 groups: (1) green-dark waters, (2) ice-floes nearby, (3) more sea-ice around, (4) no-ice, and (5) potentially affected by sub-pixel contamination.

2.2. Satellite data

Medium spatial resolution (~ 1 km) ocean color images from the MODIS sensor onboard NASA's Aqua satellite were used. MODIS Aqua provides images in the visible, NIR and shortwave infra-red. The spectral resolution of MODIS Aqua allows us to distinguish large ranges of Chl_a and organic matter concentrations with a revisiting time of 1 a 2 hours during the day over the Arctic. MODIS Aqua's 1 km spatial resolution however limits the identification of adjacent ice-edges and ice-floes.

MODIS Aqua satellite images coincident in time and space with the *in situ* data are processed with the standard AC algorithm (Bailey *et al.*, 2010). Next, for each match-up, median $\rho_w(\lambda)$ and standard deviation are calculated over a 3 by 3 pixel window around the *in situ* data location. To ensure valid match-up pairs a set of selection criteria suggested by Goyens *et al.* (2013, and references herein) were applied. Any match-up for which the time difference between satellite overpass and *in situ* measurement exceeds 3 hours is excluded and at least 6 pixels over the 3 by 3 pixel window need to be valid (i.e., not affected by clouds, sensor saturation and/or stray-light). If redundant data remain (e.g., when several measurements were taken over a surface smaller than the pixel size), the match-up with the smallest time difference is retained.

To evaluate the potential of the high spatial resolution sensor to correct medium spatial resolution images from sub-pixel and adjacent ice contamination, we used images from the recently launched Landsat 8 OLI (Operational Land Imager) sensor with 30 m spatial resolution. The revisiting time of this sensor is significantly larger relative to MODIS Aqua. Over the Arctic, Landsat-8 provides images only once a week reducing the number of available data over the region of interest. The OLI images are corrected for atmospheric effects, glint and white-caps using the AC method suggested by Vanhellemont and Ruddick (2014).

3. Results

3.1. Sea-ice contamination observed with in situ – satellite match-ups

A set of 68 match-ups were found with the MODIS Aqua images out of the 822 *in situ* data points. The 68 match-ups passed the selection criteria described in the previous section. A large amount of match-ups were excluded from data analysis because the 3 by 3 pixel window did not present at least 6 valid pixels. Figure 2 shows the satellite $\rho_w(\lambda)$ versus the *in situ* $\rho_w(\lambda)$ at 4 different wavelengths for the 68 match-ups and the 5 different classes mentioned in section 2.1. In green-dark waters, satellite retrieved $\rho_w(\lambda)$ are overestimated at 412 nm

compared to the *in situ* data. Such water masses are often encountered in the Arctic where important river discharges, rich in humic substances, release high concentrations of colored dissolved organic matter (CDOM) and nutrients that increase primary production and subsequently, Chl_a concentration. According to Fig. 2, the standard AC method tends to overestimate the signal for these water masses. This was also observed by Zibordi *et al.* (2009) and Goyens *et al.* (2013) who estimated a positive bias in the blue spectral region with the satellite estimated $\rho_w(\lambda)$ in water masses optically influenced by high CDOM and Chl_a

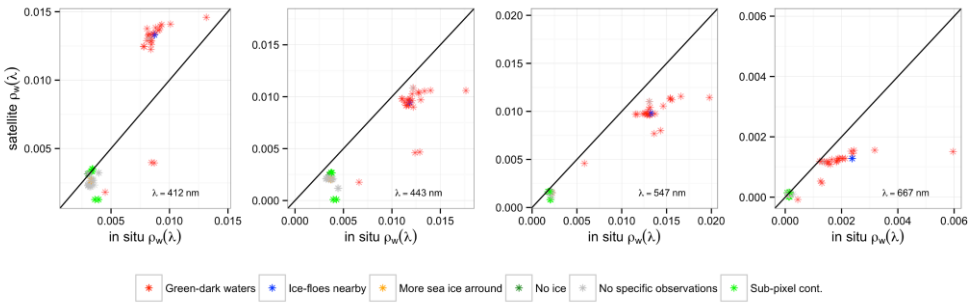

concentrations.

Fig. 2. In situ versus satellite $\rho_w(\lambda)$ for the MODIS AQUA visible bands centred at 412, 443, 547 and 667 nm and classified according to the presence of surrounding sea-ice observed during the measurement.

Nearby ice-floes were observed while taking the measurement for one match-up (blue colored point in Fig. 2). As mentioned earlier, adjacent sea-ice is expected to underestimate the water signal at 412 nm. However, these *in situ* data also indicate dark-green waters. Hence, both AC and adjacent sea-ice may result in an underestimation of $\rho_w(\lambda)$ at 412 nm. The contribution of adjacent ice-floes on the satellite retrieved $\rho_w(\lambda)$ is thus not as obvious with this data set. As shown in Fig. 2, in contrast to the adjacent sea-ice, sub-pixel contamination contributes to an underestimation of the signal, particularly in the blue spectral region. This is also in agreement with the conclusions of Bélanger *et al.*, (2007) and Wang and Shi (2009) who showed that the larger the sea-ice fraction within the satellite pixel, the more the NIR aerosol contribution will be overestimated by the AC process and, subsequently, the more $\rho_w(\lambda)$ will be underestimated at shorter wavelengths.

To further evaluate the impact of ice contamination on the satellite retrieved $\rho_w(\lambda)$, statistics have been computed for the match-ups corresponding to "green-dark waters" and "stations with some surrounding sea-ice". Figure 3 also shows the standard deviation within the 3 by 3 pixel window per class. At 412 nm relative errors range from 21 to 53% with the largest errors observed for the green-dark waters. As seen in Fig. 3, this class also shows larger standard deviations relative to the ice-contaminated match-ups. At 412 nm the green-dark waters showed a positive percentage bias of 39% while the stations with surrounding sea-ice

showed a negative percentage bias of -9%. At all other wavelengths (from 443 to 667 nm) the largest relative errors correspond to the stations with some nearby sea-ice ranging from 26% to 44%. The percentage bias remained negative for all data classes ranging from -44% to -13%. The lowest negative bias was encountered in the red spectral domain and the largest

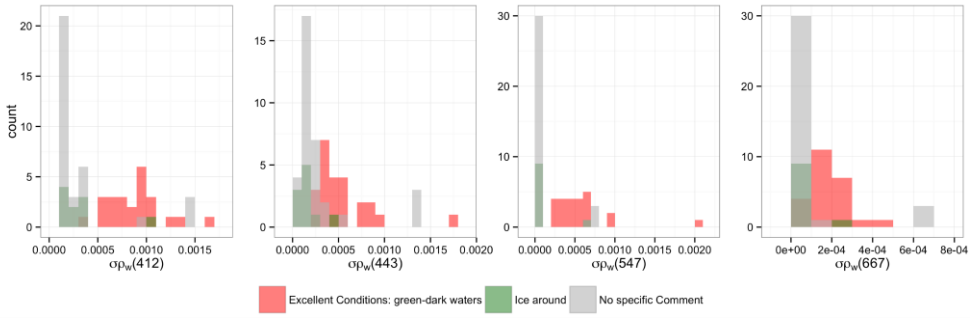

in the blue.

Fig. 3. Standard deviations of MODIS Aqua $\rho_w(\lambda)$ within the 3 by 3 pixel window at 412, 443, 547 and 667 nm.

3.1. Sea-ice contamination observed with coincident high and medium spatial resolution images

Two coincident high and medium spatial resolution image pairs were selected over the Eastern Canadian Arctic in Resolute Bay on August 11 and 13, 2014. The time differences between the acquisition of the MODIS Aqua and Landsat-8 OLI images ranged from 15 minutes to 2 hours for both pairs. The MODIS Aqua images are resampled to the resolution of the LANDSAT-8 OLI image (30 m). The first image pair shows a clear ice-edge with a few ice-floes at some distance from the coast. The second image pair covers an area affected by a set of surface variable ice-floes and a fuzzy ice-edge. Figures 4 (a-b) and (d-e) show the estimated $\rho_w(\lambda)$ at 443 nm (i.e., common visible band between MODIS Aqua and Landsat-8) for medium and high spatial resolution images, respectively. Figures 4 (c-f) show the false color images of the corresponding area where dark and bright pixels correspond to open water and sea-ice, respectively.

Overall medium spatial resolution images seem to underestimate $\rho_w(\lambda)$ compared to the high spatial resolution images (Fig. 5). This may be explained by the sub-pixel contamination resulting in an underestimation of $\rho_w(\lambda)$ in the visible spectral region. Indeed, brighter ice-covered pixels on the false color images correspond to high $\rho_w(\lambda)$ values on the high spatial resolution images but to relatively lower $\rho_w(\lambda)$ on the medium spatial resolution images. When the ice-edge is rather fuzzy (Fig. 4 (a-c)), underestimation is more obvious along the ice-edge. Note also the multiple density peaks in the medium resolution image for the fuzzy

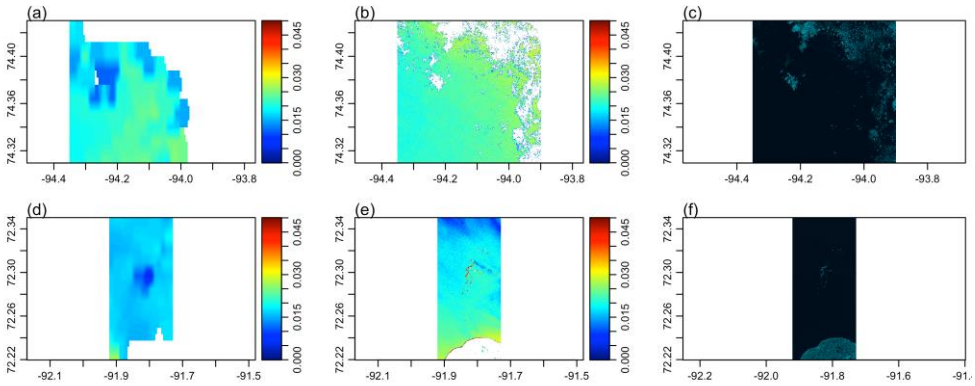

ice-edge (Fig. 5 (a)). Further effort should be done to evaluate if these peaks correspond to, for instance, differences in ice-fraction within the pixels or differences in ice-type. Along the clear ice-edge (Figs. 4 (d-f)), an overestimation of the water reflectance in the blue spectral region was expected due to adjacent ice-floes. However, this is not as apparent with the medium spatial resolution images (Fig. 4 (d-f)).

Fig. 4. MODIS Aqua resampled at 30 m spatial resolution (a, d) and Landsat-8 OLI (b, e) $\rho_w(\lambda)$ at 443 nm and Landsat-8 based false color images (c, f) for two distinctive ice-edges (fuzzy and clear ice edges, first and second column, respectively)

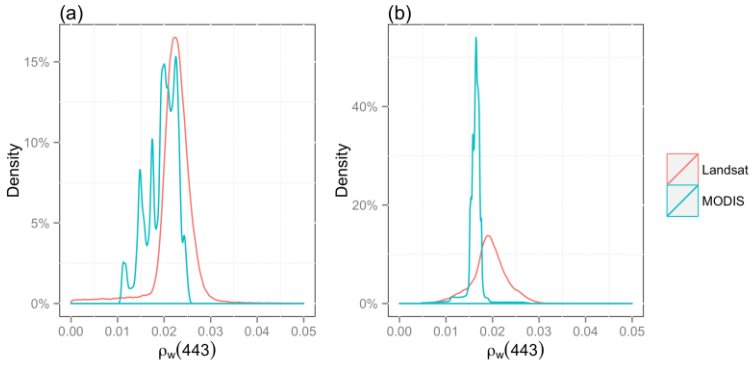

Fig. 5. Density plot of $\rho_w(\lambda)$ at 443 nm for the MODIS Aqua and Landsat images for two distinctive ice-edges; (a) fuzzy and (b) clear ice edges.

4. Conclusion and perspectives

The present study shows preliminary results in the effort to improve AC methods in icy waters. Based on a set of *in-situ*-satellite match-ups and a visual inspection of temporal and spatial coincident high and medium spatial resolution images, we attempted to evaluate sea-

ice contamination in medium spatial resolution images. Both exercises showed an obvious underestimation of $\rho_w(\lambda)$ in the blue spectral region due to sub-pixel contamination. In contrast, the adjacency effect was not as obvious. The comparison of matching high and medium spatial resolution images showed that medium resolution spatial images are significantly affected by sub-pixel sea-ice contamination. Hence, this confirms the potential to provide more accurate ice-edge ocean color data by taking advantage of the synergy between high and medium spatial resolution images. Results of the present study should be complemented by a better quantification of sea-ice contamination through, amongst other methods, the use of radiative transfer models to estimate sea-ice contamination at the top of the atmosphere (e.g., Cornet *et al*., 2009). This will be part of a future work together with a validation of high spatial resolution Landsat-8 OLI images with *in situ* data.

5. Acknowledgements

The OBPG of NASA and USGS are greatly acknowledged for the distribution of the MODIS-Aqua and Landsat-8 data and the REMSEM team from the Royal Belgian Institute of Natural Sciences for providing the Landsat ACOLITE processing tool. This work was funded by ESA through the ESA Living Planet Fellowship Program and supported by grants from the CERC in Remote Sensing of Canada's New Arctic Frontier, Takuvik Joint International Laboratory (UMI 3376 CNRS/ULaval) and ArcticNet, a Network of Centres of Excellence of Canada.

References

Antoine D., Morel A., Gordon H.R., Banzon V.F., Evans R.H. (2005). Bridging ocean color observations of the 1980's and 2000's in search of long-term trends. *Journal of Geophysical Research*, 110, C06009, doi:10.1029/2004JC002620

Bailey S. W., Werdell P. J. (2006). A multi-sensor approach for the on-orbit validation of ocean color satellite data products. *Remote Sensing of Environment*, 23, pp. 12-23.

Bélanger S., Ehn J. K., Babin M. (2007). Impact of sea ice on the retrieval of water-leaving reflectance, chlorophyll a concentration and inherent optical properties from satellite ocean color data. *Remote Sensing of Environment*, 111, pp. 51-68.

Boyce D.G., Lewis M. R., Worm B. (2010). Global phytoplankton decline over the past century. *Nature*, 466, pp. 591-596.

Cornet, L., Labonnote, C., Szczap, F. (2009). Three-dimensional Polarized Monte-Carlo Atmospheric Radiative Transfer Model (3DMCPOL): 3D Effects on Polarized Visible Reflectances of a Cirrus Cloud, *Journal of Quantitative Spectroscopy and Radiative Transfer*, 111, pp. 174-186.

Goyens C., Jamet C., Shroeder T. (2013). Evaluation of four atmospheric correction algorithms for MODIS-Aqua images over contrasted coastal waters. *Remote Sensing of Environment*, 131, pp. 63-75.

IOCCG (2015). Ocean color remote sensing in polar seas. In Babin, M., *editor*, in press, Darmouth, Canada.

Mobley C. D. (1999). Estimation of remote-sensing reflectance from above-surface measurements. *Applied Optics*, 38(36), pp. 7442-7455.

Perovich, D. K., Polashenski C. (2012) Albedo evolution of seasonal Arctic sea ice. *Geophysical Research Letter*, 39(8), L08501.

Ruddick K., Ovidio F., Rijkeboer M. (2000). Atmospheric correction of SeaWiFS imagery for turbid coastal and inland waters. *Applied Optics*, 39, pp. 897-912.

Ruddick K., De Cauwer V., Park Y.-J., Moore G. (2006). Seaborne measurements of near infrared water-leaving reflectance: The similarity spectrum for turbid waters. *Limnology and Oceanography*, 51(2), pp. 1167-1179.

Vanhellemont Q., Ruddick, K. (2014). Turbid wakes associated with offshore wind turbines observed with Landsat 8, *Remote Sensing of Environment*, 145, pp. 105-115.

Wang, M. H., Shi, W. (2009) Detection of Ice and Mixed Ice-Water Pixels for MODIS Ocean Color Data Processing. *IEEE Transactions on Geoscience and Remote Sensing*, 47, pp. 2510-2518.

Zibordi G., Berthon J.-F., D'Alimonte D. (2009). An evaluation of radiometric products from fixed-depth and continuous in-water profile data from moderately complex waters. *Journal of Atmospheric and Oceanic Technology*, 26(1), pp. 91-106.